Science Frontiers
2021; 2(2): 28-32
http://www.sciencepublishinggroup.com/j/sf
doi: 10.11648/j.sf.20210202.12

A Measurement of Micro-Porosity Formations in Titanium Alloy Fabricated Through Powder Metallurgy

Adetola Sunday Olufemi[1], Mudashiru Lateef Owowlabi[1, *], Babatunde Issa Akinola[1], Kolapo Olawale Ibrahim[2]

[1]Department of Mechanical Engineering, Faculty of Engineering and Technology, Ladoke Akintola University of Technology, Ogbomosho, Nigeria

[2]Department of Mechanical and Aerospace Engineering, Faculty of Engineering, University of Uyo, Akwa Ibom State, Nigeria

Email address:

lomudashiru@lautech.edu.ng (M. L. Owowlabi)

[*]Corresponding author

To cite this article:

Adetola Sunday Olufemi, Mudashiru Lateef Owowlabi, Babatunde Issa Akinola, Kolapo Olawale Ibrahim. A Measurement of Micro-Porosity Formations in Titanium Alloy Fabricated Through Powder Metallurgy. *Science Frontiers.* Vol. 2, No. 2, 2021, pp. 28-32.
doi: 10.11648/j.sf.20210202.12

Received: July 17, 2021; **Accepted**: July 29, 2021; **Published**: August 18, 2021

Abstract: Fractals in nature are so complicated and irregular that it is hopeless to model them by simply using classical geometry object. These fractal-like properties are found in many natural and artificial objects and processes. A new approach to describe them appropriately is the uses of fractal geometry. This geometry is successfully used in science and engineering to provide insight regarding an underlying characteristic of nature that contributes to human functioning. In this study, fractal analysis of micro-porosity distribution in titanium alloy compacted at 50, 100 and 200 MPa, sintered at 1273, 1373 and 1473 K respectively were investigated. The micro-porosities resulting from each micrograph was analyzed using weighted average and a measure of dispersion (Variance), which is done by measuring the dispersion of the shapes of the pores from that of a perfect sphere (β=1). Large-shaped macro-pores with varying degree of irregularities were observed in as-cast samples. Increased compaction pressure with sintering temperature leads to more reduction in pores. Hypothetically, the best pore shapes were found in sample compacted at 50 MPa and sintered at 1473 K. A weighted average sphericity and fractal dimension 0.7740 and 1.1889 were obtained showing that the pores are more regular in nature.

Keywords: Micro-porosity, Sphericity, Fractal Dimension, Compaction Pressure, Sintering Temperature

1. Introduction

Titanium and its alloys are relatively new engineering materials that possess an extraordinary combination of properties; relatively low density (4.5 g/cm^3), a high melting point (1668°C), and an elastic modulus of 107 GPa (15.5 × 106 psi). Titanium alloys are extremely strong: room-temperature tensile strengths as high as 1400 MPa are attainable, good yield specific strengths and low electrical conductivity makes them an excellent choice for biomedical applications [3, 10]. Titanium alloys also found applications in airplane and space vehicles, surgical implants, petroleum and chemical industries. Its low electrical conductivity contributes to the electrochemical oxidation of titanium leading to the formation of a thin passive oxide layer [10]. This protective passive layer is retained at pH values of the human body due to titanium having an oxide isoelectric point of 5 – 6 [2]. Therefore, in other to improve osseointegration, porous surface layers are usually applied [2, 14].

However, because of higher stiffness values of some metallic materials compared to human bone under load-bearing conditions, stress shielding and subsequently loosening of the implant can occur. Porous titanium alloys have emerged as implant materials that could potentially solve this problem. That is because the mechanical properties of these materials are controllable [12]. In addition to this advantage, bone tissue can grow into the pores, improving the fixation through mechanical interlocking. Such interconnected porous network also permits body fluid transportation which may enhance bone ingrowth [11].

The formation of porous Ti-10wt.%Y_2O_3 nanostructure biomaterial was studied by [11]. The powder mixture was

pressed and sintered to consolidate the granules. The sintered compacts were electrochemically etched in a mixture of H_3PO_4 and HF electrolyte at 10 V for 25 min. The electrolyte penetrates sintered samples through the grain boundaries, resulting in effective material removal and pores formation. It was found that the pore diameter reaches up to 50 µm, which is very attractive for strong bone bonding. Samples of titanium powder with the addition of natural polymers (corn starch, rice starch, potato starch and gelatin) at proportion of 16 wt.% were studied by [13]. The pores obtained with the addition of potato and corn starches lead to homogenous and well distributed structure.

Samples obtained from addition of rice starch and gelatin formed macro-pores that are randomly distributed within the structure. The apparent porosity for all samples was near 40%. The processing technique allowed the open pore formation in which the macro-pores mimic the trabecular bone structure and allows the bone-implant anchorage. Similarly, [14] studied the biocompatible alloying elements of niobium (Nb) and zirconium (Zr) prepared by a space-holder sintering method. Their study revealed that the porous TiNbZr scaffold with a porosity of 69% exhibits a mechanical strength of 67 MPa and an elastic modulus of 3.9 GPa, resembling the mechanical properties of cortical bone.

The developed of porous Ti with directional pores was examined by [7]. In their study, porosity of the material increased with increasing number of Mg wires and decreased with increasing sintering temperature and compaction pressure. The most advantageous point of the novel fabrication process employed in their study was that both porosity of the material and the diameter of the pores were controlled by the number of Mg wires, the sintering temperature and the compaction pressure. They concluded that the material developed have superior osteogenesis properties which can be used as possible bone implants possessing. In this study, fractal analysis was employed to numerically characterize the micro-pores distribution in Ti-alloys developed by [7].

2. Methods

In the study conducted by [7], commercial pure Ti powders (99.9 mass.%) with a particle size of 20µm and Mg wires (99.9 mass.%) with a diameter of 250µm were prepared. A stainless steel cylindrical disk 8 mm diameter and 4 mm thickness was filled with the powders, and three wires were horizontally placed with the bottom of the disk into the powders. Samples were then compacted at a pressure of 50, 100 and 200 MPa into the disk. Subsequently, sintering experiment was carried out in a vacuum at 1273, 1373 and 1473 K respectively. All compacts were heated to the sintering temperature at a heating rate of 10 K/min, held for 2 hours and then annealed to room temperature. In addition, a mold made of stainless steel with holes placed at the wall side was designed and Ti powders (99.9 mass.%) with a particle size of 50 µm and Mg wires with a diameter of 400 µm were used to fabricate porous Ti with directional pores. The morphology of the sintered samples has obtained by [7] is clearly shown in Figure 1, which revealed high porosity level and exhibiting high degree of agglomeration.

3. Microstructural Characterization

Fractal depletion of microstructures in Figure 1 above was depicted in Figure 2. There is significant concentration of irregular pores geometries consisting of smaller particles at the onset of sintering (Figures 2a, b and c) above which the pores are partially distributed within the micrograph.

Fractal geometry has been known for many years as a mathematical concept introduced by [9]. Its tools were applied successfully to characterize irregularly shaped and complex Figures by a mathematical value wherever Euclidean geometry fails. One of the advantages of fractal analysis is the ability to quantify the irregularity and complexity of objects with a measurable value called the fractal dimension (a common tool in physics and image processing). Fractal analysis has been used by many researchers to numerically describe complex microstructures including graphite flakes, nodules and pores [1, 4–6, 8].

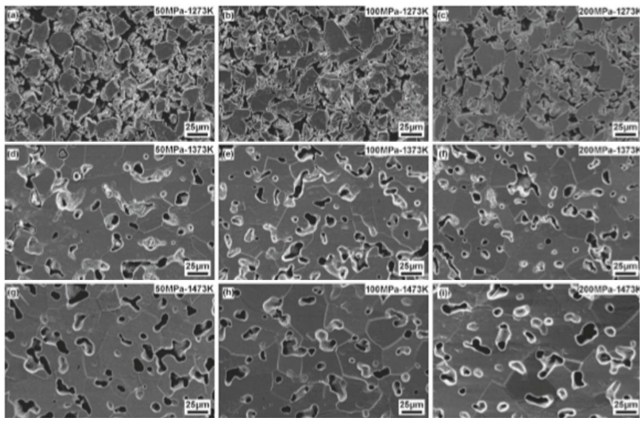

Figure 1. *SEM of the microstructure for micro-pores dispersed in porous Ti after sintering at the sintering temperature of (a, b, c) 1273K; (d, e, f) 1373K and (g, h, i) 1473K. The compact pressure were (a, d, g) 50MPa; (b, e, h) 100MPa and (c), (f), (i) 200MPa.*

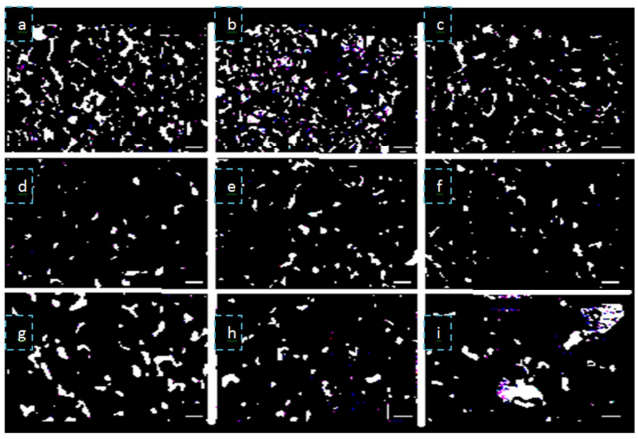

Figure 2. *Isolation of micro-pores within the micrograph.*

In this work, the mathematical basis for measuring chaotic objects with the power law was adopted. The basic equation is as follows:

$$P=P_e\,\delta^{D-1}\ (1 < D < 2 \text{ and } \delta_m < \delta < \delta_M) \quad (1)$$

where "P_e" is the measured perimeter, "P" is the true perimeter, "δ" is the yardstick, "δ_m and δ_M" are the upper and lower limits respectively for any shape and "D" is defined as the fractal dimension. The fractal dimension "D" describe the complexity of the contour of an object which can be more practically called roughness. Sphericity "β", on the other hand is used with fractal dimension "D", to describe the shape of the pore sizes formed [1, 9]. It can be expressed as:

$$\beta=4\pi A_T/P^2\ (0 < \beta < 1 \text{ and } 1 < D < 2) \quad (2)$$

From the above two equations:

$$\beta=(4\pi A_T/P^2)\,\delta^{2(1-D)}\ (0 < \beta < 1 \text{ and } 1 < D < 2) \quad (3)$$

where "A_T" is the total pore size area. When β=1 and D=1, a perfect circular shape is formed by the pore sizes in the microstructure. As β decreases, the shapes become more elongated showing a departure from perfect sphere.

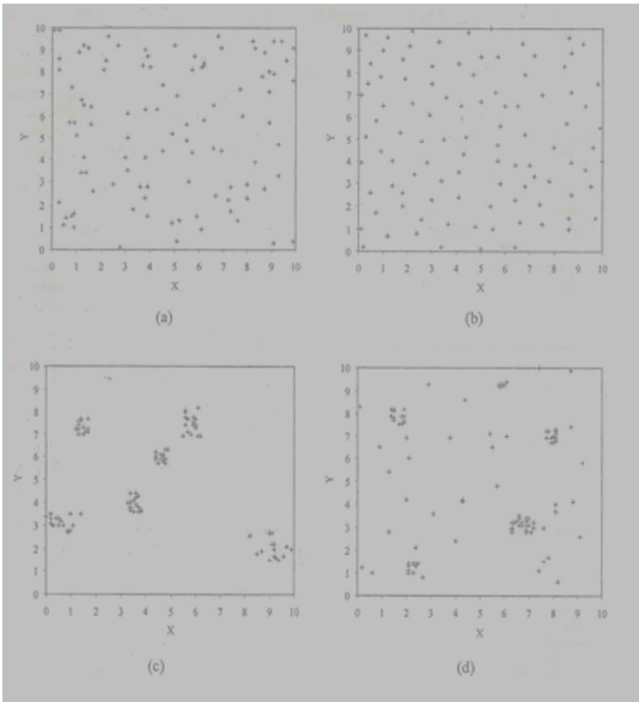

Figure 3. *The four common types of spatial point patterns (a) random, (b) regular (c) clustered, (d) clustered superimposed on random background.*

In this study, an interactive Matlab program was developed to obtain the numerical values of the fractal dimension "D" and the sphericity "β". Box counting method was used with a counter incorporated into the program and the small boxes or pixels occupied by the pores outlines were counted. In all, four pixels (2×2 pixels, 4×4 pixels, 8×8 pixels and 16×16 pixels) and four grid sizes (200×200, 100×100, 50×50 and 25×25) were selected. The selections were made for better resolution and to obtain accurate results. The spatial point pattern method (Figure 3) and the pore size distribution map (Figure 4), were used to describe the patterns displayed by the micro-pore sizes after the samples had been sintered. The micro-pore size distribution map can further be used to identify the shapes of the pores and their dispersion from regular shapes.

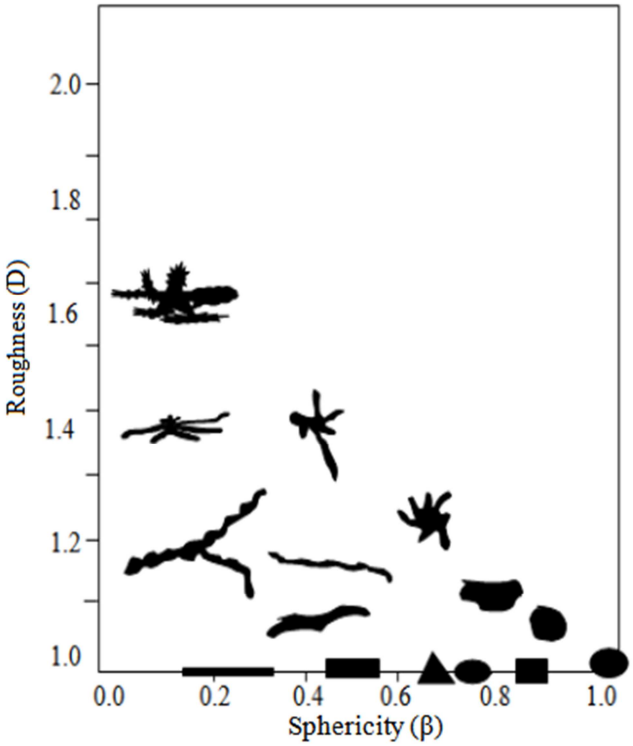

Figure 4. *Illustration of development of irregular shapes based upon Euclidean circle or rectangle.*

4. Results and Discussion

Presented in Figures 5-13 show the micro-porosity distribution maps as obtained from the fractal analysis of each respective micrographs. Each data point represents an individual pore and the big-sized data point is the weighted average of the pores' sphericities and fractal dimensions respectively. In Figure 5, the micro-porosity distribution map dispersed in porous Ti compacted at 50 MPa and sintered at 1273 K. The weighted average has 0.6597 and 1.2968 values for sphericity and fractal dimension. The pores are clustered superimposed on random background. Figure 6 is the Ti sample compacted at 100 MPa and sintered at 1273 K. The weighted average values of 0.7064 and 1.2657 for sphericity and fractal dimension were obtained. The pores are clustered superimposed on random background. Also presented in Figure 7 is the sample compacted at 200 MPa, sintered at 1273 K. Weighted average sphericity and fractal dimension of 0.6917 and 1.3201 were obtained. The pores are said to be clustered superimposed on random background.

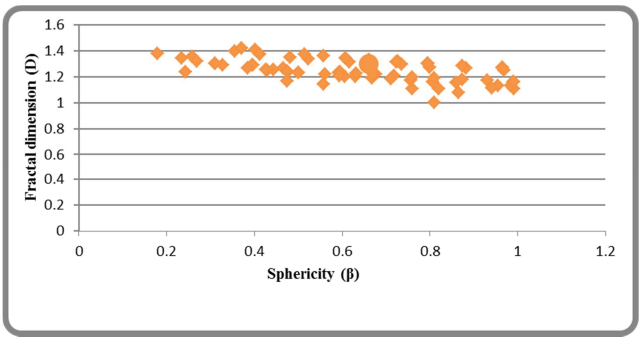

Figure 5. *Micro-porosity distribution map for porous Ti compacted and sintered at 50MPa and 1273K.*

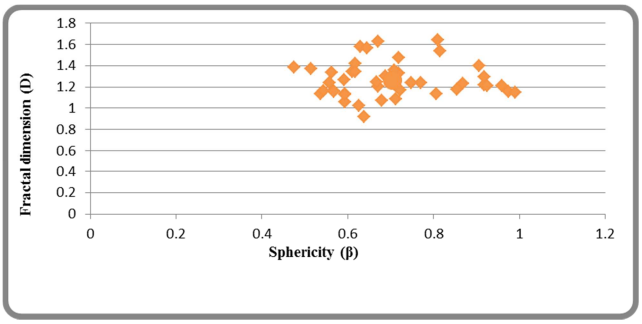

Figure 6. *Micro-porosity distribution map for porous Ti compacted and sintered at 100MPa and 1273K.*

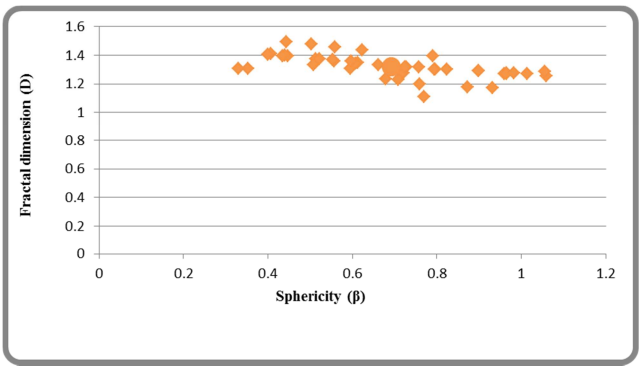

Figure 7. *Micro-porosity distribution map for porous Ti compacted and sintered at 200MPa and 1273K.*

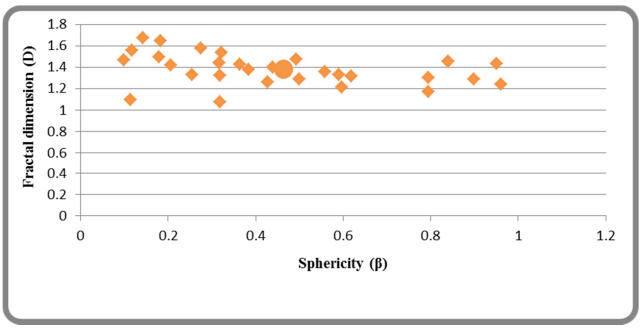

Figure 8 *Micro-porosity distribution map for porous Ti compacted and sintered at 50MPa and 1373K.*

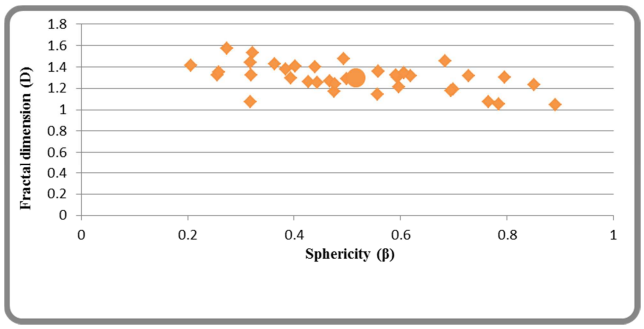

Figure 9. *Micro-porosity distribution map for porous Ti compacted and sintered at 100MPa and 1373K.*

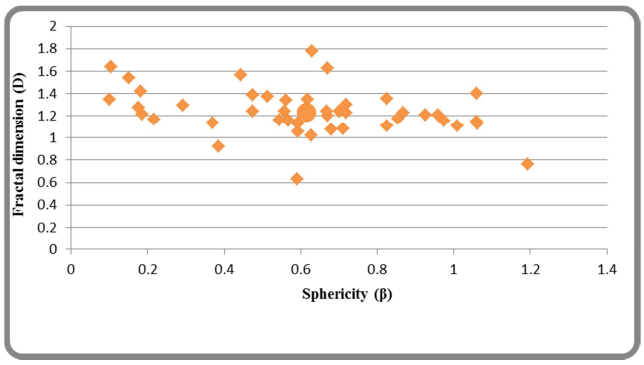

Figure 10. *Micro-porosity distribution map for porous Ti compacted and sintered at 200MPa and 1373K.*

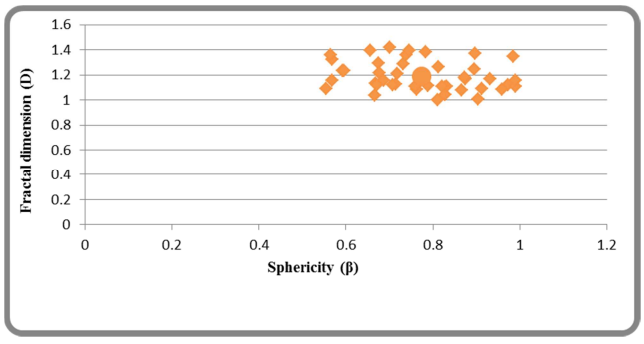

Figure 11. *Micro-porosity distribution map for porous Ti compacted and sintered at 50MPa and 1473K.*

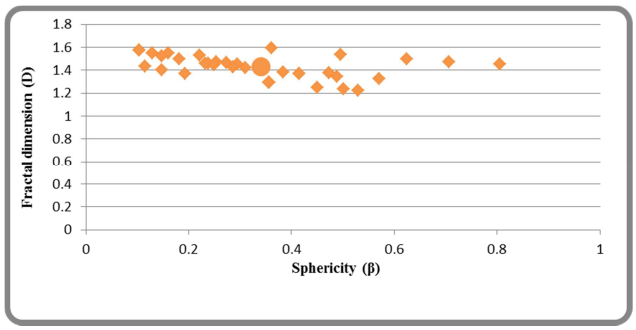

Figure 12. *Micro-porosity distribution map for porous Ti compacted and sintered at 100MPa and 1473K.*

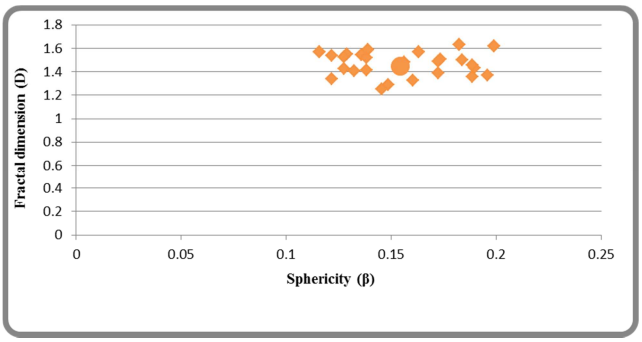

Figure 13. *Micro-porosity distribution map for porous Ti compacted and sintered at 200MPa and 1473K.*

Presented in Figure 8 is the micro-porosity distribution map dispersed in porous Ti compacted at 50 MPa and sintered at 1373 K. Weighted average sphericity and fractal dimension of 0.4634 and 1.3799 were obtained. The pores are more randomly distributed and regular. In Figure 9, a weighted average sphericity and fractal dimension 0.5165 and 1.2998 were obtained. The pores are randomly distributed. Also observed in Figure 10 is a weighted average sphericity and fractal dimension 0.6146 and 1.2319. The pores are said to be randomly distributed. Presented in Figure 11 is the sample compacted 50 MPa and sintered at 1473 K. A weighted average sphericity and fractal dimension 0.7740 and 1.1889 were obtained. The pores are more regular, clustered and superimposed on random background.

5. Conclusion

The micro-porosity distribution map in Figure 13 was characterized with low and high values of β and D. However, the porosity distribution map dispersed in porous Ti-alloy in Figures 5 to 9 have pores with their sphericities largely distributed within 0.2 and 1.0. It is noteworthy that high compaction rate does not favor the distribution of micro-porosity within the Ti-alloy.

Acknowledgements

Authors thankfully acknowledge Lee et al. (2013), members of Division of Materials Science and Engineering, Inha University, Korea, for privilege in making use of parts of their work.

References

[1] Durowoju, M. O. and Akintan, A. L. (2013). Variation between Fractal Geometry and Mechanical Properties of Al Alloys under Different Heat Treatments. *International Journal of Science and Advanced Technology*, 3 (4): 11-21.

[2] Elias, C. N., Lima, J. H. C., Valiev, R. and Meyers, M. A. (2008). Biomedical applications of titanium and its alloys. *Journal of The Minerals, Metals and Materials Society,* JOM, 60 (4): 6–49.

[3] Guo, S., Qu, X., He, X., Zhou, T. and Duan, B. (2006). Powder injection molding of Ti-6Al-4V alloy. *Journal of Material Processing Technology*, 173, 310–314.

[4] Hangai, Y. and Kitahara, S. (2008). Quantitative Evaluation of Porosity in Al Die Castings by Fractal Analysis of Perimeter. *Materials Transactions*, 49 (4): 782–786.

[5] Huang, Y. J. and Lu, S. Z. (2002). A Measurement of The Porosity in Aluminum cast Alloys Using Fractal Analysis. *Proceeding of 2nd International Aluminum Casting Technology Symposium*, ASME, Houston U.S.A.

[6] Kong, J., Xu, C., Li, J., Chen, W. and Hou, H. (2011). Evolution of fractal features of pores in compacting and sintering process. *Advanced Powder Technology*, 22, 439–442.

[7] Lee, J., Lee, J., Kim, M. and Hyun. (2013). Fabrication of Porous Titanium with Directional Pores for Biomedical Applications. *Materials Transactions*, 54 (2): 137–142.

[8] Lu, S. and Hellawell, A. (1995). Fractal Analysis of Complex Microstructures in Materials.

[9] Mandelbrot, B. B. (1982). The fractal geometry of nature. New York: W. H. Freeman and Co.

[10] Sidambe, A. T., Figueroa, I. A., Hamilton, H. G. C. and Todd, I. (2012). Metal injection moulding of CP-Ti components for biomedical applications. *Journal of Material Processing Technology*, 212, 1591–1597.

[11] Montasser, D., Adamek, G., Jakubowicz, J. and Khalil, K. A. (2014). Fabrication, Microstructure and Properties of Mechanically Alloyed and Electrochemically Etched Porous Ti-Y_2O_3 *International Journal Electrochemical Science*, 9, 7773–7783.

[12] Ryan, G., Pandit, A. and Apatsidis, D. P. (2006). Fabrication methods of porous metals for use in orthopaedic applications. *Biomaterials*, 27 (13): 2651–2670.

[13] Tamiye, S. G., Kalan, B. V., José, C. B. and Ana, H. A. B. (2013). Mimicking Bone Architecture in a Metallic Structure. *Advances in Science and Technology*, 84: 7–12.

[14] X. Wang, Li. Yuncang, D. H. Peter and C. Wen, "Biomimetic Modification of Porous TiNbZr Alloy Scaffold for Bone Tissue Engineering, in: Materials Transactions, 16 (1): 25-44, 2010.